Excitons and band structure of highly anisotropic GaTe single crystals

Aishi Yamamoto, Atsushi Syouji, and Takenari Goto
Physics Department, Graduate School of Science, Tohoku University, Aoba-ku, Sendai 980-8578, Japan

Erkin Kulatov
General Physics Institute, Russian Academy of Sciences, Vavilov str. 38, Moscow, Russia

Kaoru Ohno* and Yoshiyuki Kawazoe
Institute for Materials Research, Tohoku University, Aoba-ku, Sendai 980-8577, Japan

Kazuhito Uchida and Noboru Miura
Institute for Solid State Physics, University of Tokyo, 5-1-5 Kashiwa-no-ha, Kashiwa 277-8581, Japan
(Received 16 January 2001; published 28 June 2001)

Exciton characteristics of GaTe single crystals grown by vapor-phase transport were studied by optical measurements. A hydrogenlike exciton series up to $n=4$ was clearly observed in the absorption spectra at 2 K. In the $n=1$ exciton energy region three types of exciton lines were found. By analyzing microphotoluminescence and micro-Raman-scattering spectra on the basis of group theory, it was clarified that these exciton lines are not due to different polytypes but to intrinsic exciton states. Furthermore, optical-absorption spectra in a magnetic field at 4.2 K were measured. In the Voigt configuration, one and two components for $E\|b$ and $E\perp b$ polarizations, respectively, were observed in the $n=1$ and 2 exciton lines. These magnetic-field dependencies cannot be interpreted on the basis of the previously proposed L-S coupling regime. The electronic band structure of GaTe was studied by the *ab initio* tight-binding linear muffin-tin orbitals method. It was found that GaTe is a direct-gap semiconductor and that the band edge is located at an *M* point of the Brillouin zone. From a comparison of exciton absorption spectra and the calculated band structure, the existence of the three types of excitons was interpreted from the viewpoint of *j-j* coupling. Our model calculation was also able to explain the Zeeman splitting and the diamagnetic shift of the exciton peak energies.

DOI: 10.1103/PhysRevB.64.035210 PACS number(s): 68.35.Ja, 71.35.Ji

I. INTRODUCTION

Most III-VI compound semiconductors, such as GaSe, GaS, and InSe, have a layered structure. Because of the anisotropy and polytypism of these materials, their optical properties have been studied extensively.[1] Conversely, the optical properties and even band structure of GaTe, which is one of the III-VI compound semiconductors, are less well known. One of the reasons is that GaTe crystallizes in a more complicated structure than do other III-VI compounds.

The crystal structure of GaTe has been investigated by Pearson.[2] One layer has two kinds of Ga-Ga bonds: One lies perpendicular to the layer, similar to GaSe, and the other lies in the layer. The crystal symmetry is monoclinic with the space group C_{2h}^3. Generally, in layered materials, the main symmetry axis is perpendicular to the layer plane. However, there is no such symmetry axis in GaTe, and only one twofold symmetry axis exists in the direction parallel to the *b* axis, which is in the layer plane.

Irwin *et al.*[3] reported Raman-scattering and infrared-absorption spectra of GaTe, and they reported that no conjugate mode (lattice vibrations of in- and out-phase modes) was observed. This result means that the primitive cell of GaTe has only one layer; i.e., there is no polytypism. When the crystal has some polytypes, the exciton states become complicated, and hence, the polytypism makes study of the precise excitonic properties difficult. In this sense, GaTe is an excellent material to study the excitonic properties of layered structures.

Although GaTe is a material of low symmetry, Camassel *et al.*[4] reported that the optical properties near the band-gap energy region are very simple and that there is no significant anisotropy in the absorption spectrum. Wan *et al.*[5] studied photoluminescence (PL) and transmission spectra, and they found that the lowest excitonic state splits into two levels, X_1 and X_2. The X_1 exciton was observed only for polarization $E\perp b$, while the X_2 exciton was observed for both polarizations $E\perp b$ and $E\|b$. They interpreted X_1 and X_2 as being singlet and triplet excitons, respectively, from the viewpoint of L-S coupling.[5] Although the transmission spectra reported by them are not clear, the oscillator strengths of X_1 and X_2 seem to be almost the same. This fact contradicts their assignment, because the triplet exciton is optically forbidden. Recently, they reconsidered the origins of X_1 and X_2.[6] Although their explanation is inconsistent, they suggested that X_1 and X_2 for $E\|b$ are due to singlet excitons constructed from heavy- and light-hole bands, respectively. However, X_2 for $E\perp b$ is a triplet state, and their assumption still contradicts the experimental results. The purpose of the present study was to clarify the origins of X_1 and X_2 states. For this purpose, we synthesized single GaTe crystals and studied various optical properties such as absorption, PL, micro-PL, micro-Raman, and absorption in a magnetic field. The experimental setup is described in Sec. II, and the experimental results are presented in Sec. III. In Sec. IV the electronic band structure calculated by the *ab initio* tight-binding scalar-relativistic linear muffin-tin orbitals (TB-LMTO)

method is presented, and then the origin of the excitons is discussed in detail.

II. EXPERIMENTAL SETUP

The samples used in this study were grown by a vapor-growth technique.[7] The same molecular weights of 6N gallium metal (purchased from Nilaco Co.) and 6N tellurium (purchased from Rare Metallic Co., Ltd.) were sealed in a quartz ampule in vacuum. They were reacted at 870 °C for 1 h and then kept at 820 °C for one week. Many flakelike single crystals were grown in the quartz ampule. The sample crystallinity was checked by x-ray diffraction measurement. The crystal *b*-axis, which is along the growth direction, can be determined easily. We selected transparent as-grown crystals and attached them stress free to a sample holder. The typical size of these samples was 1 mm$\times$3 mm$\times$0.5 μm.

A tungsten lamp was used as a probe light source for the absorption measurements, and a 514.5-nm light from an NEC GLS3200 Ar ion laser was used as an excitation light for the PL measurements. The absorption and PL spectra were obtained using a Jobin-Yvon T64000 triple monochromator with a charge-coupled device (CCD) camera.[8] Each sample was immersed in pumped liquid helium to be cooled to about 2 K. An optical microscope was also used for micro-PL and micro-Raman measurements.

For the studies of absorption spectra under a magnetic field, two experimental setups were used: a superconducting magnet for a low-magnetic field up to 7 T, and a nondestructive-type pulse magnet for a high-magnetic field up to 40 T. For measurements in low-magnetic fields, a white light from a tungsten lamp was used as a probe light, and the transmitted light was analyzed using a Jobin-Yvon T64000 triple monochromator equipped with a CCD camera. Each sample was immersed in pumped liquid helium to be cooled to about 2 K. For measurements in a high magnetic field, a white light from a xenon flash lamp transmitted through the sample immersed in liquid helium was dispersed by a Jobin-Yvon HR-320 monochromator and detected by a CCD camera.[9] In both experiments, the magnetic-field B was applied parallel to the crystal b axis ($B\|b$), and the absorption spectra were measured in both $E\|b$ and $E\perp b$ polarizations.

III. EXPERIMENTS

A. Absorption and photoluminescence spectra

The absorption and PL spectra of GaTe are shown by solid lines and dashed lines, respectively, in Fig. 1. The upper and lower curves are for the polarizations $E\perp b$ and $E\|b$, respectively. A Wannier-type exciton series up to $n=4$ can be clearly observed in the absorption spectra. In both the absorption and PL spectra, two peaks X_1 and X_2 can be seen at around the $n=1$ exciton energy region in the $E\perp b$ polarization, and one peak X_2 is observed in the $E\|b$ polarization. The polarization dependence and spectral shape of PL spectra are almost the same as those previously reported.[5] The Stokes shifts of both the X_1 and X_2 peaks are about 0.1 meV. Such a very small shift indicates that they are due to free

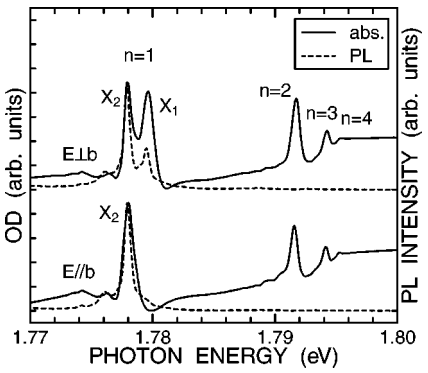

FIG. 1. Absorption (solid lines) and PL (dashed lines) spectra of GaTe at 2 K. Upper and lower spectra shows the polarizations $E\perp b$ and $E\|b$, respectively.

exciton states. There exists a small PL peak at around 1.776 eV whose intensity depends on the sample. Wan *et al.*[5] reported that this PL originates from the exciton bound to a localized state induced by the strain in the sample. In the absorption spectrum for $E\perp b$, X_1 and X_2 have almost the same oscillator strengths. Therefore, X_2 is not related to a triplet state, which is dipole forbidden. Figure 2 shows more precise absorption structures in the $n=1$ (a) and $n=2,3$ (b) exciton energy regions. The solid and dashed lines show the spectra for $E\perp b$ and $E\|b$ polarizations, respectively. Since the sample used in the experiment for which the results are shown in Fig. 2 was thinner than that used in the experiment for which the results are shown in Fig. 1, the interference effect of excitonic polariton makes the spectra a little complicated. Figure 2(a) shows that the peak energies of X_2 for

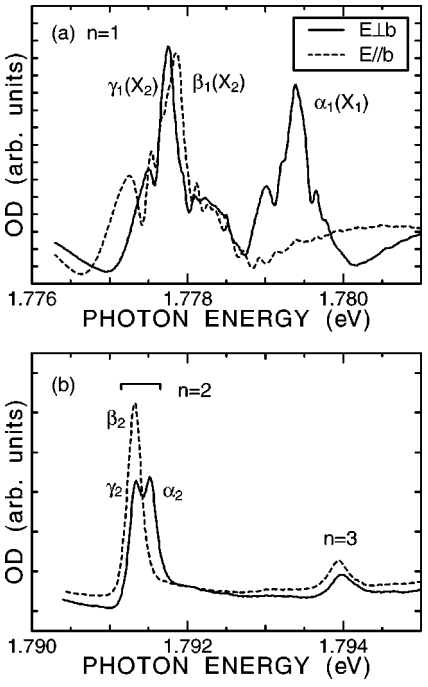

FIG. 2. Precise absorption spectra of $n=1$ (a) and $n=2$, 3 (b) exciton energy regions at 2 K. The solid and dashed lines correspond to the polarizations $E\perp b$ and $E\|b$, respectively.

TABLE I. Observed and reported exciton energies and calculated exciton binding energies R_0 and energy gap Eg in meV. The estimated $n=1$ exciton energies by using R_0 and Eg are also shown in parentheses.

	α	β	γ	X_1 [a]	X_2 [a]
$n=1$	1779.39±0.02	1777.85±0.02	1777.75±0.02	1779.7	1778.5
(calc.)	(1778.0)	(1777.2)	(1777.2)		
$n=2$	1791.52±0.02	1791.32±0.02	1791.32±0.02	1792.0	
$n=3$	1794.04±0.03	1793.95±0.02	1793.95±0.02	1794.4	
R_0	18.1±0.4	18.9±0.3	18.9±0.3	15.6	17.6
E_g	1796.06±0.07	1796.05±0.06	1796.05±0.06	1796	

[a]Reference 5.

the two polarizations are slightly different. The character table of C_{2h} symmetry[10] shows that all of the irreducible representations are one dimensional; i.e., there is no degeneracy, and hence, the X_2 peaks for the two polarizations are thought to be due to different states. Furthermore, it can be seen that $n=2$ exciton for $E\perp b$ splits into two peaks. These facts suggest that *there are three exciton series* in the absorption spectra. Consequently, X_1, X_2 $(E\|b)$, and X_2 $(E\perp b)$ are now denoted as α_1, β_1, and γ_1, respectively, where the subscript indicates a principal quantum number of the exciton states *n*.

Table I shows exciton peak energies obtained from our work and those of previous studies for comparison. The exciton binding energies R_0 and band-gap energies E_g are also shown in the table. In general, the observed $n=1$ exciton energy shows a discrepancy from the simple expression of E_g-R_0 because the average distance between electron and hole of the $n=1$ exciton is rather small and a static dielectric constant cannot be used for calculating Coulomb force. Consequently, R_0 and E_g were calculated from $n=2$ and 3 exciton energies in this study. Since the exciton energies of β_n and γ_n $(n\geqslant 2)$ are the same, the calculated energies of E_g are identical. The values of E_g for the three exciton series are the same within the experimental error. This fact indicates that these exciton series are *constructed from the same electron and hole bands.* As will be mentioned in the next section, it should be noted that the observed exciton peak energies are sensitive to an inner strain and shift within 3 meV. The exciton peak energies shown in Table I were obtained from Fig. 2. Unfortunately, the exciton energies of $n=4$ could not be determined because of the small absorption intensity.

B. Micro-PL and micro-Raman measurements

In layered materials, a polytypism generally appears due to the difference in the stacking sequence. When the crystal has some polytypes, the energies of exciton states, especially $n=1$ exciton states, of the polytypes are slightly different.[1] This fact suggests that the three exciton series originate from the polytypism. Irwin *et al.*,[3] however, have reported Raman-scattering and infrared-absorption spectra of GaTe in which no conjugate mode is observed. This result means that the primitive cell of GaTe has only one layer; i.e., there is no polytypism. To confirm their results, we measured position dependence of micro-PL and micro-Raman spectra with a spacial resolution of 1 μm.

Figure 3 shows typical Raman spectra under $z'(yy)\bar{z'}$ and $z'(x'y)\bar{z'}$ configurations at 18 K, where x' and y are in the layer plane defined through $y\|b$ and $y\perp x'$, and z' is normal to the layer plane. The irreducible representations of phonon modes at the center of the Brillouin zone (BZ) for C_{2h} symmetry are described by

$$\Gamma = 12\mathrm{Ag}+6\mathrm{Bg}+6\mathrm{Au}+12\mathrm{Bu}. \tag{3.1}$$

Raman active modes are 12 Ag and 6 Bg modes, which are allowed for $z'(yy)\bar{z'}$ and $z'(x'y)\bar{z'}$ configurations, respectively. Among the Raman active modes, 11 Ag and 3 Bg modes have been reported by Irwin *et al.*[3] and Abdullaev *et al.*[11] The numbers indicated in Fig. 3 correspond to the phonon modes numbered by them. The inset shows the precise spectra of the energy region of mode 13. It has a shoulder in the lower-energy side. We fitted this spectrum by the sum of two Lorentzians, which is shown by the solid curve. The dashed lines show the two Lorentzians, and we numbered them 13 and 13' from the higher energy side. As shown in Fig. 3, we obtained one Ag and one Bg modes denoted 13'

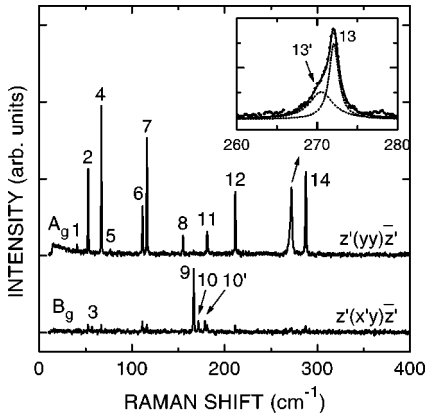

FIG. 3. Raman-scattering spectra of GaTe crystal at 18 K under the configurations of $z'(yy)\bar{z'}$ and $z'(x'y)\bar{z'}$ which correspond to A_g and B_g symmetries, respectively. The inset shows precise spectra of the energy region of mode 13. The solid line shows a fitting curve assuming two Lorentzians. The fitted two Lorentzians are separately shown by dashed lines.

TABLE II. Observed Raman-active phonon symmetries and energies (cm^{-1}). Previously reported values are also listed.

Feature number	Symmetry	Present work (± 0.3 cm^{-1})	Irwin[a] (± 2 cm^{-1})	Abdullaev[b] (± 2 cm^{-1})
1	Ag	40.9	41	41
2	Ag	52.8	52	53
3	Bg	57.1	58	57
4	Ag	67.1	67	67
5	Ag	76.6	76	76
6	Ag	111.3	110	110
7	Ag	116.2	115	115
8	Ag	155.2	155	153
9	Bg	166.6	164	163
10	Bg	171.8	170	169
10'	Bg	178.8		
11	Ag	181.2	178	177
12	Ag	211.5	208	210
13	Ag	270.5	271	271
13'	Ag	272.1		
14	Ag	287.5	284	284

[a]Reference 3.
[b]Reference 11.

and 10', respectively; i.e., all Ag modes are observed, although there are two unobserved Bg modes. There are some unnumbered peaks in the lower spectrum that are thought to be Ag modes. Forbidden Ag modes are presumably observed in the $z'(x'y)\overline{z'}$ configuration, because of a small misalignment in the experimental setup. Table II shows the observed phonon modes and previously reported data for comparison. If the sample has a polytype, there is a possibility to observe zone-folded modes of acoustic phonons[12] in the energy region lower than 30 cm^{-1}. As was also reported by Irwin *et al.*,[3] however, no such phonon mode was observed, indicating that GaTe has no polytype. We also measured the position dependence of the Raman spectra, and no significant change was observed.

Figure 4 shows a map of the PL spectra obtained by moving the laser spot relative to the sample position at intervals of 5 μm with $E\perp b$ polarization. Two main peaks, α_1 and

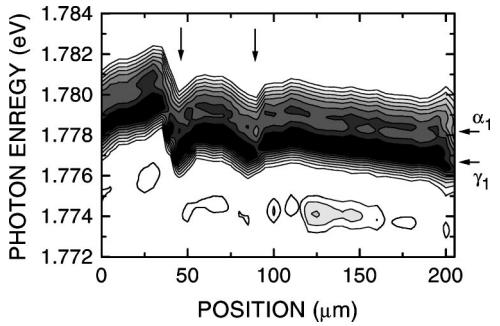

FIG. 4. Position dependence of the PL spectra at 18 K. The PL peak positions of α_1 and γ_1 excitons are indicated by the arrows. The two downward pointing arrows shows the positions of domain boundaries of the GaTe crystal.

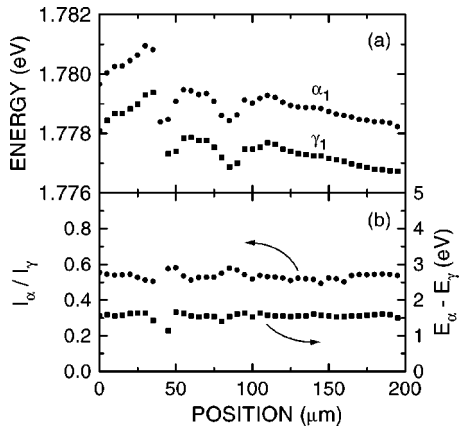

FIG. 5. (a) Position dependence of peak energies of α_1 and γ_1. (b) Position dependence of the peak intensity ratio (I_α/I_γ) and peak energy difference ($E_\alpha - E_\gamma$).

γ_1, are indicated by arrows. The two peak energies are plotted as a function of the position in Fig. 5(a). The position dependence of the PL intensity ratio (I_α/I_γ) and energy difference ($E_\alpha - E_\gamma$) of α_1 and γ_1 are also shown by circles and squares, respectively, in Fig. 5(b). If the α_1 and γ_1 are due to different polytypes and the density ratio of the polytypes depends on the sample position, the PL intensity ratio is thought to be changed by the sample position. As is shown in Fig. 5(b), however, the PL intensity ratio does not depend on the sample position, and hence, polytypism is not thought to exist. On the other hand, the peak energies of the two excitons continuously shift without changing the energy difference between α_1 and γ_1. This energy change is thought to be due to a small spacial difference in inner strain. We notice discontinuities shown by the downward pointing arrows in Fig. 4. These positions correspond to boundaries of the crystal domain, which can be seen in the microscopic real image. The crystal domains have different inner strains, which presumably cause the discontinuities of the PL map image.

C. Magnetic-field dependence of absorption spectra

Absorption spectra for $E\|b$ and $E\perp b$ in various magnetic fields at 4.2 K are shown in Figs. 6(a) and 6(b), respectively. In the lowest spectrum for a zero magnetic field, a Wannier-type exciton series can be seen up to $n=3$. Figure 7 shows the absorption peak energies as a function of the magnetic field. The closed and open circles correspond to $E\perp b$ and $E\|b$ polarizations, respectively. If β_1 and γ_1 are triplet states and the g value is assumed to be the same as that of GaSe, $g=2.7$,[1] the energy splitting under 40 T is estimated to be 6 meV. The spectral resolution is sufficient to observe this splitting of the triplet state, if this state exists. With increasing magnetic field, however, no paramagnetic splitting is observed. This result also suggests that the exciton state of X_2 (β_1 and γ_1) is not the triplet state. Magnetic-field dependence clearly differs between β_1 and γ_1 excitons. As was stated in Sec. III A, it is obvious that β and γ are different states.

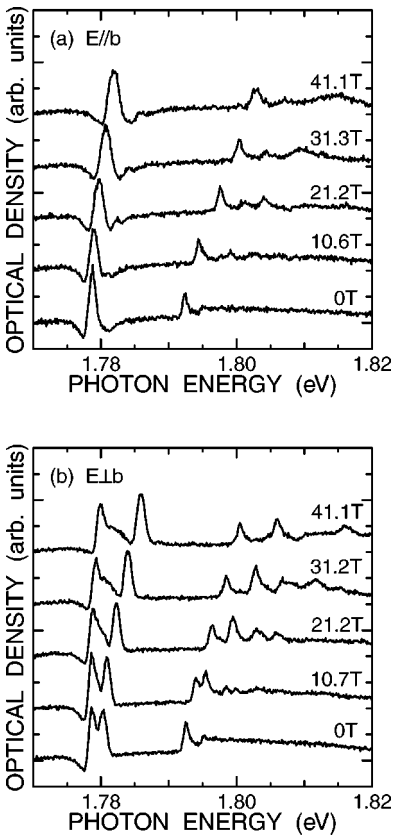

FIG. 6. Magnetic-field dependence of the absorption spectra at 4.2 K. The applied magnetic fields are indicated in the figure. The polarizations of the incident light are $E\|b$ (a) and $E\perp b$ (b). Exciton series α_n, β_n, and γ_n ($n=1$ and 2) are denoted.

IV. DISCUSSION

In order to understand the origin of the three exciton series, we calculated the band structure and its density of states (DOS) of a GaTe crystal. The electronic band structure was studied by the *ab initio* TB-LMTO method. The calculations and results are described in Sec. IV A. In Sec. IV B the origin of the exciton series is discussed in detail.

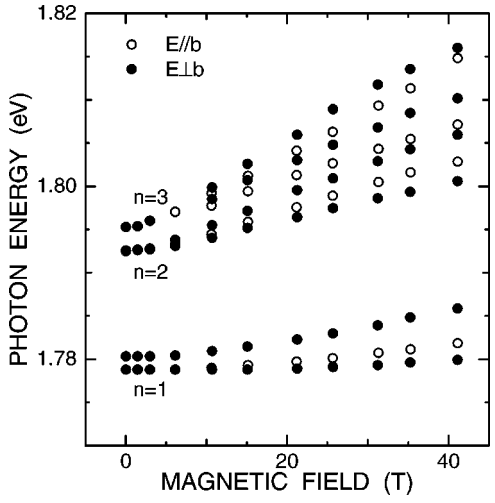

FIG. 7. Peak energies of three types of exciton series as a function of the magnetic field. The closed and open circles correspond to $E\perp b$ and $E\|b$ polarizations, respectively.

TABLE III. Crystal structure parameters of GaTe.

Legend	x-param.	z-param.
$Ga_1(4i)$	0.781 71	0.919 10
$Ga_2(4i)$	0.559 45	0.800 60
$Ga_3(4i)$	0.019 46	0.582 70
$Te_1(4i)$	0.980 54	0.822 26
$Te_2(4i)$	0.287 07	0.827 36
$Te_3(4i)$	0.605 33	0.448 74
$E_1(2a)$	0.0	0.0
$E_2(4i)$	0.275 59	−0.349 41
$E_3(4i)$	0.332 23	0.353 06
$E_4(4i)$	0.191 24	−0.100 42
$E_5(4i)$	0.498 50	−0.084 83
$E_6(4i)$	0.152 93	0.402 93
$E_7(8j)$	0.106 34	−0.260 81
	$y=0.2629$	
b-axis unique	c-axis unique	
$a=17.404$ Å	$a=17.404$ Å	
$b=4.077$ Å	$b=4.077$ Å	
$c=17.930$ Å	$c=10.456$ Å	
$\hat{\beta}=145.61°$	$\hat{\beta}=104.44°$	

A. Electronic band structure

1. Details of the calculation

Gallium telluride crystallizes into a monoclinic structure made up by a set of layers bound by weak van der Waals interaction with atoms at the special positions shown in Table III.[13] The unit cell contains 12 molecules of GaTe, but the primitive cell contains only six molecules within each layer. The gallium atoms occupy three sets of $4i$ positions (Ga_1,Ga_2,Ga_3), and three types of tellurium atoms (Te_1,Te_2,Te_3) also exist at $4i$ positions. Here, $(4i)$, $(2a)$, $(8j)$ in Table III are Wyckoff positions.

As in other layered semiconductors, *intra*layer bonds are mainly covalent with some ionic contribution, and *inter*layer bonds are of a weak van der Waals type. The main interatomic bonds within each layer of a GaTe crystal are arranged to give a fundamental unit, where each gallium atom is surrounded by another gallium atom and by three tellurium atoms. Each tellurium atom, in turn, is linked to three nearby gallium atoms, and, in addition, supplies the weaker interlayer bond with other tellurium sites facing it from the adjacent layer.

Electronic structure calculations of GaTe were done by using the TB-LMTO method in atomic-spheres-approximation (ASA) including combined correction.[14] Exchange and correlation contributions to crystalline potential were included through the von Barth-Hedin local density approximation (LDA) (Ref. 15) to the density functional theory.[16,17]

In our open structure under consideration and with only atom-centered spheres, the ASA would cause substantial er-

rors, either due to a large overlap and misrepresentation of the potential or due to the neglect of charge in the van der Waals gap mentioned above. Therefore, it is necessary to pack the van der Waals gap with interstitial (empty) spheres. In general, the requirements for choosing the sphere positions and radii are that the superposition of spherical potentials approximate the full three-dimensional potential as close as possible, so that the overlap error for the kinetic energy is acceptable and that the entire charge is inside the spheres. The positions of the interstitial spheres are chosen among the nonoccupied symmetry positions of the space group. This procedure was carried out automatically using a computer program.[18] The band structure is not very sensitive to the relative sphere radii.

The results showed that five types of interstitial spheres are placed at the $4i$ positions (total number, 10) and that one empty sphere is at the $2a$ position in the origin of the frame reference shown in Table III. All of the above-mentioned spheres are situated inside the layer on the face of the primitive unit cell. Four further interstitial spheres are placed at the $8j$ positions just between the layers in the van der Waals gap. Therefore, the primitive unit cell contains 12 real atoms (six Ga atoms and six Te atoms of three types each) and 15 fictitious interstitial spheres of seven types.

The TB-LMTO basis set consists of Ga ($4s$ and $4p$) and Te ($5s$ and $5p$), and the interstitial empty sphere consists of $1s$ and $2p$ LMTO's, or so called ''low orbitals.'' The Ga ($4d$) and Te ($5d$ and $4f$) and interstitial $3d$ partial waves (''intermediate orbitals''), $\phi_{Rl}(\varepsilon,r)$, were taken at the fixed energies $\varepsilon_{\nu Rl}$, which are the centers of gravity of the occupied parts of the *Rl* projected bands, and were included only in the tails of the above-mentioned LMTO's.

All **k**-space integrations were performed by the tetrahedron method.[19] For complex crystal structures, it is important to control and manage the process of stabilization of the self consistent iterations. Convergence to self-consistency was achieved with a mesh of 372 irreducible **k** points for the monoclinic lattice and was checked through the total energy, which was stable within 1 μRy at the last successive iterations towards self consistency. To generate the densities of states (DOS), we used 775 **k** points in 1/4 (C_{2h}^3) irreducible parts of BZ.

In monoclinic crystals two primitive unit cells with various centerings can be chosen: ''*b*-axis unique'' and ''*c*-axis unique'' (see Table III). We performed TB-LMTO benchmark calculations for these two centerings and found that the electronic structures were practically identical.

2. Electronic structure

Figure 8 shows the calculated TB-LMTO energy bands in several directions in the monoclinic BZ for GaTe. The energy zero is taken at the highest occupied level. It can be seen from Fig. 8(b) that most bands have a weak dispersion in the plane perpendicular to the $\mathbf{k}_y$ axis reflecting the strongly two-dimensional layered structure of GaTe.

We obtained a direct band gap of 1.13 eV at the *M* point, or equivalently at the *P* point, which is about 37% smaller than the experimental value, 1.796 eV. Here, the *M* and *P*

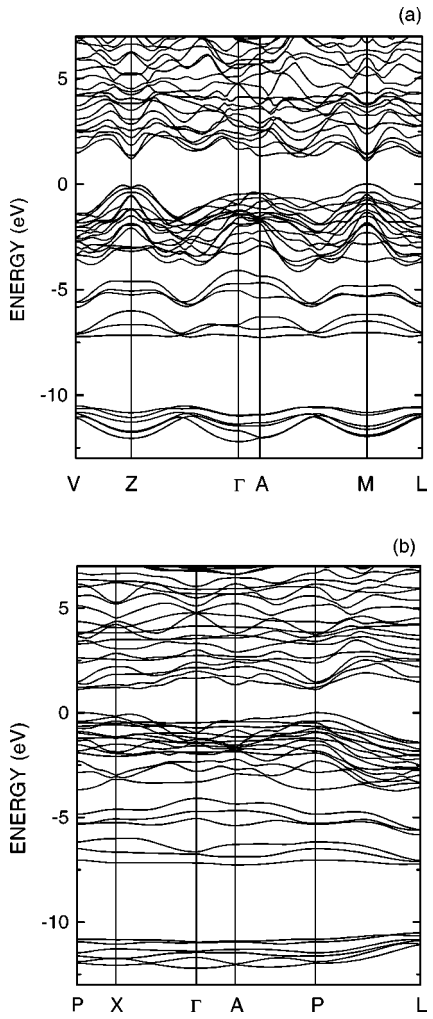

FIG. 8. (a) and (b) Band structure of GaTe crystal along high-symmetry directions in the monoclinic BZ.

points are defined as $1/2(-\vec{G}_1+\vec{G}_2+\vec{G}_3)$ and $1/2(\vec{G}_1+\vec{G}_2+\vec{G}_3)$, respectively, where $\vec{G}_1$, $\vec{G}_2$, and $\vec{G}_3$ are reciprocal lattice vectors of (0.41474, −1.0, 0), (0.41474, 1.0, 0), and (0.33221, 0, 0.22738), respectively, in the unit of $2\pi/b$. Underestimation of the band gap energy is well known and is common to all LDA calculations. The calculated band gap can be improved by using the computationally intensive GW method.[20] However, the GW technique becomes prohibitively time consuming when it is applied to complex systems such as low-symmetry crystals with many atoms per unit cell.

The valence band consists of four groups of bands. The lowest portion of the valence band (six bands extending from −12.2 to −10.5 eV) is composed of Te $5s$ states, with some covalent admixtures of Ga $4s$ states, and a smaller contribution due to Ga $4p$ states. This part of the valence band is split off from the upper part of the valence band by an energy difference of about 3.3 eV, due to the effect of the strong Te ion potential on its own *s*-like states. The next two upper portions of the valence bands (six bands in the range from −7.2 to −4.2 eV) consist predominantly of Ga $4s$ states with significant contributions of Te $5p$ states and with

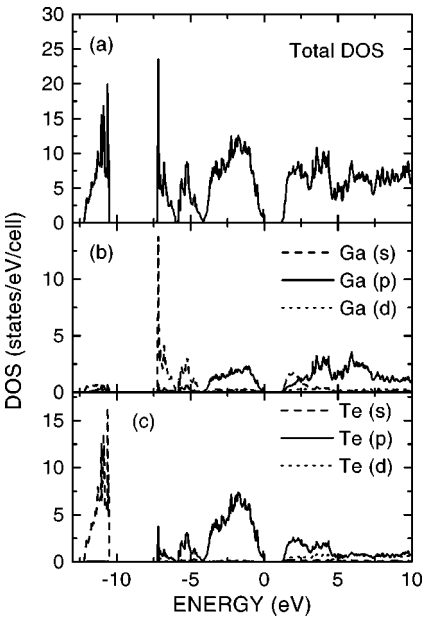

FIG. 9. (a) Total DOS of GaTe crystal. (b), (c) Partial DOS's of Ga and Te, where the *s*, *p*, and *d* components of those atoms are shown by the dashed, solid, and dotted lines, respectively.

some admixtures of Te $5s$ and Ga $4p$ states. The highest group of bands (15 bands from -4.2 eV to 0 eV) is formed mainly by highly hybridized Te $5p$ and Ga $4p$ states with small contributions due to Ga $4s$ and $4d$ states. The states at the valence-band edge originate completely from Te $5p$ and Ga $4p$ states. The low-energy conduction bands (from 1.13 eV to 3 eV) are mixtures of comparable contributions from Te $5p$, Ga $4s$, and $4p$ states with somewhat smaller contributions of Ga $4d$ states and Te $5d$ states at the conduction-band edge.

The total DOS is depicted in Fig. 9 along with the local partial DOS of Ga and Te. Note that DOS show a quasigap at about -4.2 eV, which was found in ultraviolet photoelectron spectroscopy (UPS).[21] Three UPS features visible in the 0 to -4 eV region and two other UPS peaks in the -5 to -8 eV region are in qualitative agreement with the calculated DOS's.

From the above calculations, we found that GaTe is a direct-gap semiconductor and that the band gap is located at the *M* point. If there is more than one equivalent *M* point in the first BZ, intervalley scattering might occur, and this would cause energy splitting of excitons as was observed in TlCl.[22] The symmetry of the *M* point is C_{2h}, which is the same as that of the Γ point. This means that the *M* point has only one star, and thus, there is only one valley in the first BZ. Therefore, the possibility of intervalley scattering is excluded.

B. Origin of the three excitons

As we described in the previous sections, there appears three optically allowed exciton series, i.e., α, β, and γ in GaTe, which are constructed from the same conduction and valence bands. The results of band-structure calculation indicated that GaTe is a direct-gap semiconductor and that the band gap is located at the *M* point. From these experimental and theoretical aspects, we will discuss here the origin of the three exciton series.

In a similar III-VI compound semiconductor, GaSe, exciton states are interpreted in a *L-S* coupling regime,[1] which seems to be different from the case of GaTe. Here, we pay attention to the fact that the spin-orbit splitting energy of a Te atom, 589 meV, is larger than that of a Se atom, 247 meV.[23] Therefore, not the *L-S* coupling regime but the *j-j* coupling regime is expected to be suitable for an interpretation of the exciton states in GaTe. Consequently, we will explain the exciton states in terms of the *j-j* coupling scheme.

From the results of band-structure calculation, the band-gap exciton is assumed to be the optical transition mainly from *p* (Ga $4p$ and Te $5p$) to *s* (Ga $4s$) orbital states at the *M* point. By introducing spin functions, they are described as $s\uparrow_e$ and $s\downarrow_e$ for conduction bands and $-(p_x+ip_z)\uparrow_h + p_y\downarrow_h$ and $(p_x-ip_z)\downarrow_h+p_y\uparrow_h$ for valence bands. The *y* axis is defined parallel to the crystal symmetry *b* axis. Here, *s* stands for a wave function transforming like *s*-type atomic states; p_x, p_y, and p_z are wave functions transforming like p_x-, p_y-, and p_z- type atomic states; and $\uparrow_{e(h)}$ and $\downarrow_{e(h)}$ represent the up and down spin functions of an electron (hole), respectively. We assume that the p_y component strongly mixes with p_x and p_z components due to the large spin-orbit interaction of a Te atom. The mixing coefficients of the *p* orbital functions are included in the functions. As was described in the previous section, the symmetry of the *M* point is C_{2h}, which is the same as that of the Γ point. Thus, we use the notation of Γ point for convenience hereafter. According to the coupling coefficients table for C_{2h},[10] four wave functions of the excitons formed by the above electron and hole states are described as

$$\begin{aligned}
\psi_1^{-1} &= s(-p_x\chi_1 - p_z\chi_3 + p_y\chi_s),\\
\psi_2^{-1} &= s(-p_x\chi_3 + p_z\chi_1 + p_y\chi_2),\\
\psi_3^{-2} &= s(p_x\chi_s - p_z\chi_2 + p_y\chi_1),\\
\psi_4^{-2} &= s(p_x\chi_2 + p_z\chi_s + p_y\chi_3),
\end{aligned} \tag{4.1}$$

where the superscript of the wave functions ψ corresponds to the representation in the C_{2h} symmetry group. In Eqs. (4.1), χ_s is a spin function of a spin singlet state, and χ_1, χ_2, and χ_3 are spin functions of the spin triplet states. In the C_{2h} symmetry, these are described as

$$\begin{aligned}
\chi_s &= (\uparrow_e\downarrow_h - \downarrow_e\uparrow_h)/\sqrt{2},\\
\chi_1 &= (\uparrow_e\uparrow_h + \downarrow_e\downarrow_h)/\sqrt{2},\\
\chi_2 &= i(\uparrow_e\downarrow_h + \downarrow_e\uparrow_h)/\sqrt{2},\\
\chi_3 &= i(\uparrow_e\uparrow_h - \downarrow_e\downarrow_h)/\sqrt{2}.
\end{aligned} \tag{4.2}$$

Since the functions of ψ_1^{-1}, ψ_3^{-2}, and ψ_4^{-2} have a singlet component (χ_s), they are optically allowed, while ψ_2^{-1} is a

pure triplet state and optically forbidden. In C_{2h} symmetry, Γ_1^- and Γ_2^- states are optically allowed for $E\|b$ and $E\perp b$, respectively. Thus, the ψ_1^{-1} state is allowed for $E\|b$, and ψ_3^{-2} and ψ_4^{-2} states are allowed for $E\perp b$. If the wave functions of ψ_4^{-2}, ψ_1^{-1}, and ψ_3^{-2} correspond to the experimental exciton series α, β, and γ, respectively, they satisfy the selection rule. Here, we define the pure triplet state ψ_2^{-2} as ε.

The Zeeman term in the Hamiltonian is written as

$$H=\frac{\mu_B}{\hbar}(\hat{l}_e+g_e\hat{s}_e)\mathbf{B}-\frac{\mu_B}{\hbar}(\hat{l}_h+g_h\hat{s}_h)\mathbf{B}, \tag{4.3}$$

where $\mu_B=e\hbar/2m$ is the Bohr magneton, $\hat{l}_{e(h)}$ and $\hat{s}_{e(h)}$ are orbital and spin angular momentum operators, respectively, and $g_{e(h)}$ is a g factor of an electron (hole). In the $B\|b$ configuration, α and γ states and β and ε states mix with each other. The energies of the diagonalized exciton states are

$$V_\pm=[E_\beta+E_\varepsilon\mp\sqrt{(E_\beta-E_\varepsilon)^2+4H^*HB^2}]/2+\sigma\frac{5n^4+n^2}{6}B^2 \tag{4.4}$$

$$W_\pm=[E_\alpha+E_\gamma\mp\sqrt{(E_\alpha-E_\gamma)^2+4F^*FB^2}]/2+\sigma\frac{5n^4+n^2}{6}B^2,$$

where E_α, E_β, E_γ, and E_ε are exciton energies of α, β, γ, and ε at $B=0$, respectively, and σ is a diamagnetic coefficient. In Eq. (4.4) a diamagnetic shift is also considered. The asterisk refers to a conjugate complex. The parameters H and F are defined by $H=A+C+D$ and $F=A+C+D^*$, where

$$\begin{aligned} A&=i|s|^2(|p_x|^2+|p_z|^2)\mu_B,\\ C&=-ig_h|s|^2(|p_x|^2+|p_z|^2-|p_y|^2)\mu_B/2,\\ D&=ig_e|s|^2(|p_x|^2+|p_z|^2+|p_y|^2)\mu_B/2. \end{aligned} \tag{4.5}$$

Here, $|s|$ and $|p_\xi|$ $(\xi=x,y,z)$ are expected values of s and p_ξ functions, respectively.

Figure 10(a) shows the energies of $n=1$ exciton peaks as a function of the magnetic field. The solid lines represent the fit using Eq. (4.4). The fitting parameters are $|F|$, $|H|$, and σ. From the energy shift of α_1 and γ_1, we obtain $|F|=(7.0\pm0.1)\times10^{-5}$ eV/T and $\sigma=(2.03\pm0.03)\times10^{-6}$ eV/T^2. If the value of $|H|$ is not small, β and ε states are mixed with each other, and the ε state becomes optically allowed. However, no ε state was observed in our experiment. This result means that the mixing is not significant and that the value of $|H|$ is small. It is reasonable to assume that the value of $|H|$ is negligibly small because the energy shift of β_1 can be fitted using only the diamagnetic coefficient σ. The value of σ is common for the solid lines for α_1 and γ_1. Using the obtained values of σ and exciton binding energy R_0 shown in Table I, the exciton reduced mass, effective dielectric constant, and exciton Bohr radius were estimated, and evaluated values are shown in Table IV.

In the above consideration, we assume that the magnetic fields are in a weak-field regime; i.e., the ratio of cyclotron energy to exciton binding energy is sufficiently smaller than unity. This value equals unity when the magnetic fields are

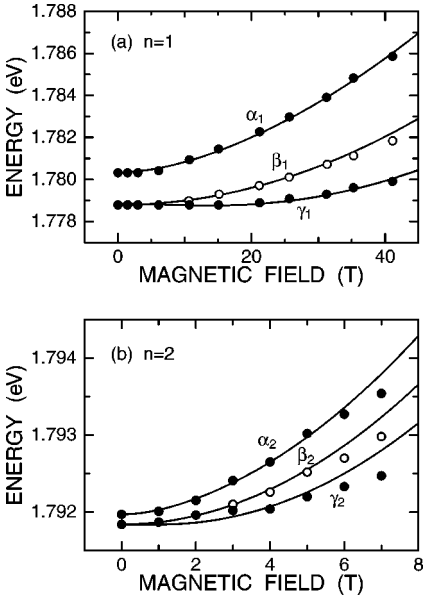

FIG. 10. Peak energies of $n=1$ (a) and $n=2$ (b) excitons as a function of the magnetic field. The closed and open circles correspond to $E\perp b$ and $E\|b$ polarizations, respectively. The solid lines represent the fit using Eq. (4.4) with adjustable parameters $|F|=7.0\times10^{-5}$ eV/T, $|H|=0$ eV/T, and $\sigma=2.03\times10^{-6}$ eV/T^2.

70.6, 17.6, and 7.8 T for $n=1$, 2, and 3 excitons, respectively. For $n=1$ exciton, the whole range of the magnetic fields studied here is in the weak-field regime, and the calculated curves fit well to the experimental data. To satisfy the limitation of the $n=2$ excitons, we consider the range of magnetic fields lower than 17.6 T. Figure 10(b) shows the energies of the $n=2$ exciton peaks as a function of the magnetic field in a weak-field regime. The solid curves show the calculated results of Eq. (4.4) using the same values of F, $H(=0)$, and σ as those obtained for the $n=1$ excitons. The calculated curves agree well with the experimental points, which proves the suitability of our model.

We discuss here why the energies of α_1 and γ_1 excitons are different ($\sim$1.5 meV). The x and z axes are located at the plane normal to the b axis, though their directions cannot be defined. Therefore, the polarizations of the dipole moments of both α_1 and γ_1 excitons are not known. If the polarization direction of γ_1 is assumed to lie in the layer plane and perpendicular to the b axis, γ_1 is a pure transverse exciton, while α_1 is a pure longitudinal exciton. In this assumption, the energy difference between α_1 and γ_1 excitons is thought to be due to longitudinal-transverse splitting. However, the longitudinal exciton is not optically allowed, and hence, only the γ_1 exciton is expected to be observed. This is not the case. Therefore, this assumption is too simple

TABLE IV. Excitonic parameters obtained by using σ and R_0, where m_0 is a free-electron mass.

Reduced mass	$(0.209\pm0.004)m_0$
Dielectric constant	12.3 ± 0.2
Bohr radius	31.1 ± 0.3 Å

to explain the experimental results. We think both α_1 and γ_1 excitons are longitudinal-transverse mixed excitons: α_1 and γ_1 are longitudinal-like and transverselike excitons, respectively. In other words, these two excitons become optically allowed due to the low crystal symmetry.

We noticed similar behavior of the $n=1$ exciton state in PbI_2 crystals under a magnetic field.[9] The crystal symmetry of 2H-PbI_2 is D_{3d}. The lowest exciton state is constructed from an A_4^+ valence hole and an A_4^- conduction electron.[24] The symmetries of the exciton states can be described as $A_1^+ \times A_4^+ \times A_4^- = A_1^- + A_2^- + A_3^-$. Here, A_2^- and A_3^- are allowed transitions for $E \| c$ and $E \perp c$ polarizations, respectively, while A_1^- is a pure triplet state, where c is perpendicular to the layer plane. When the magnetic field is applied in the direction perpendicular to the c axis, the crystal symmetry is reduced to C_{2h}. Due to the lower crystal symmetry, three types of excitons become observable for $E \perp c$ polarization (Fig. 7 in Ref. 9). They are a longitudinal exciton (A_2^-) and two transverse excitons (A_3^-) showing Zeeman splitting. The triplet exciton A_1^- becomes optically allowed due to a mixing with a singlet component. In GaTe the crystal symmetry is C_{2h}, which is the same as that of PbI_2 under a magnetic field $B \perp c$. The four observed exciton states, A_2^-, A_3^-, and A_1^- in PbI_2, are thought to correspond to α, β, γ, and ε for GaTe, respectively. However, an ε state is not observed because of the small mixing coefficient with the β state.

V. CONCLUSION

In summary, we have synthesized thin single crystals of GaTe by a vapor-growth technique and measured absorption, PL, micro-PL, and micro-Raman spectra. Three exciton series were observed near the band edge, and the exact exciton binding energies and band-gap energy were determined. The band structure of GaTe was calculated, and it was found that GaTe is a direct-gap semiconductor and that the band gap is located at the M point. It is concluded that observed excitons are associated with j-j coupled, optically allowed exciton states. Our model explains the existence of three optically allowed excitons and the selection rules for the polarizations. Furthermore, magnetic-field dependence of the exciton peak energies are also explained by our model. From this study, some of the excitonic parameters have been determined.

ACKNOWLEDGMENTS

The authors are grateful to Professor O. Jepsen for providing us with the TB-LMTO program. Computations were performed at the Supercomputing Center of the Institute for Materials Research, Tohoku University. One of the authors (E.K.) acknowledges the financial support from the Materials Design Virtual Laboratory (donated by IBM and Hitachi) at the Institute for Materials Research, Tohoku University. This work was partly supported by the Russian Fund of Basic Investigations, Grant No. 98-02-016133-a, and the Russian Federal Program ''Integration,'' Grant No. K0 573.

*Present Address: Department of Physics, Yokohama National University, 79-5 Tokiwadai, Hodogaya-ku, Yokohama 240-8501, Japan.

[1] See for example, E. Mooser and M. Schlüter, Nuovo Cimento Soc. Ital. Fis., B **18**, 164 (1973); M. Schlüter, *ibid.* **13**, 313 (1973).

[2] W. B. Pearson, Acta Crystallogr. **17**, 1 (1964).

[3] J. C. Irwin, B. P. Clayman, and D. G. Mead, Phys. Rev. B **19**, 2099 (1979).

[4] J. Camassel, P. Merle, and H. Mathieu, Physica B **99**, 309 (1980).

[5] J. Z. Wan, J. L. Brebner, R. Leonelli, and J. T. Graham, Phys. Rev. B **46**, 1468 (1992); see also, J. Z. Wan, J. L. Brebner, R. Leonelli, G. Zhao, and J. T. Graham, *ibid.* **48**, 5197 (1993); J. Z. Wan, J. L. Brebner, and R. Leonelli, *ibid.* **52**, 16 561 (1995); **53**, 15 413 (1996).

[6] J. Z. Wan, F. H. Pollak, J. L. Brebner, and R. Leonelli, Solid State Commun. **102**, 17 (1997).

[7] A. Syouji, A. Yamamoto, and T. Goto, Phys. Rev. B **60**, 15 519 (1999).

[8] A. Yamamoto, A. Syouji, and T. Goto, J. Lumin. **87-89**, 207 (2000).

[9] Y. Nagamune, S. Takeyama, and N. Miura, Phys. Rev. B **43**, 12 401 (1991).

[10] G. F. Koster, J. O. Dimmock, R. G. Wheeler, and H. Statz, *Properties of the Thirty-Two Point Groups* (MIT Press, Cambridge, MA, 1963).

[11] G. B. Abdullaev, L. K. Vodopyanov, K. R. Allakhverdiev, L. V. Golubev, S. S. Babaev, and E. Y. Salaev, Solid State Commun. **31**, 851 (1979).

[12] See for example, S. Nakashima, H. Katahama, Y. Nakakura, and A. Mitsuishi, Phys. Rev. B **31**, 6531 (1985).

[13] *Pearson's Handbook, Desk Edition, Crystallographic Data for Intermetallic Phases*, Vol. 2, edited by P. Villars (ASM International, The Materials Information Society, Materials Park, 1997); M. Julien-Pouzol, S. Jaulmes, M. Guittard, and F. Alapini, Acta Crystallogr., Sect. B: Struct. Crystallogr. Cryst. Chem. **35**, 2848 (1979).

[14] O. K. Andersen and O. Jepsen, Phys. Rev. Lett. **53**, 2571 (1984); O. K. Andersen, O. Jepsen, and D. Glotzel, in *Highlights of Condensed-Matter Theory*, edited by F. Bassani, F. Fumi, and M. P. Tosi (North-Holland, New York, 1985).

[15] U. von Barth and L. Hedin, J. Phys. C **5**, 1629 (1972).

[16] P. Hohenberg and W. Kohn, Phys. Rev. **136**, B864 (1964).

[17] W. Kohn and L. J. Sham, Phys. Rev. **140**, A1133 (1965).

[18] G. Krier, O. Jepsen, A. Burkhardt, and O. K. Andersen, The TB-LMTO-ASA Program, Max-Planck-Institut fuer Festkoerperforschung, 1995.

[19] P. Bloechl, O. Jepsen, and O. K. Andersen, Phys. Rev. B **49**, 16 223 (1994).

[20] L. Hedin, Phys. Rev. **139**, A796 (1965).

[21] R. H. Williams, I. T. McGovern, R. B. Murray, and M. Howells, Phys. Status Solidi B **73**, 307 (1976).

[22] E. Mohler, G. Schlögl, and J. Treusch, Phys. Rev. Lett., **27**, 424 (1971); C. Uihlein and J. Treusch, Solid State Commun. **17**, 685 (1975); S. Kurita, K. Kobayashi, and Y. Onodera, Suppl. Prog. Theor. Phys. **57**, 10 (1975).

[23] *Atomic Energy Levels*, edited by C. E. Moore, Natl. Bur. Stand. (U.S.) Circ. No. 467 (U.S. GPO, Washington, D.C., 1958), Vol. 2 (for Se) and Vol. 3 (for Te).

[24] I. C. Schlüter and M. Schlüter, Phys. Rev. B **9**, 1652 (1974).